Spatial Calibration for 3D Freehand Ultrasound via Independent General Motions

Qianqian Cai[1], Jian-yu Lu[2], Chang Peng[1], Juan C. Prieto[3], Alan J. Rosenbaum[3], Jeffrey S. A. Stringer[3], Xiaoning Jiang[1]
[1]Department of Mechanical and Aerospace Engineering, North Carolina State University, Raleigh, NC, United States
[2]Department of Bioengineering, The University of Toledo, Toledo, OH, United States
[3]Division of Global Women's Health, Department of Obstetrics and Gynecology, The University of North Carolina - Chapel Hill, Chapel Hill, NC, United States

***Abstract*—The concept of 3D freehand ultrasound has been of great interest to researchers for decades due to many advantages over conventional 2D ultrasound, such as image quality that is less dependent on a sonographer's skills and more intuitive and interactive 3D views of scanned objects. However, obstacles such as the need for spatial calibration remain, which hinder the effective application of this technique in clinical settings. Here we report the feasibility and accuracy of performing spatial calibration based upon a closed-form solution to matrix equations formed by two independent general motions. We achieved millimeter-level accuracy for translational and degree-level accuracy for rotational degrees of freedom. The calibration accuracy may be further improved by optimizing the matrix solution.**

***Keywords*—3D freehand ultrasound, spatial calibration, optical tracking, closed-form solution**

I. Introduction

A. Background

To acquire intuitive and real-time ultrasound (US) images with high-quality, three dimensional (3D) freehand US technique has attracted much research attention in recent years. This method permits reconstruction of 3D structures of the imaging object by determining the positions and orientations of successive two dimensional (2D) US images based on a tracked 2D US probe [1]. Popular tracking sensors that meet the accuracy requirements of the probe tracking include mechanical arms, electromagnetic sensors, and optical sensors [2]. Most tracking systems require markers or receivers to be attached to the tracking objects, but because these may not be attached to the US imaging plane, they are usually attached to the probe surface. This causes a discrepancy between the US image tracjectory and tracked probe motion due to a lever effect at the reference [3]. Thus, a spatial calibration that transforms the probe motion to the US image motion is essential to obtain an accurate reconstruction and visualization of the scanned object.

The relative spatial relationship is fixed between the marker set attached to the US probe and US imaging plane if the marker set is stationary and the imaging setting remains the same. Therefore, the goal of spatial calibration is to ascertain that fixed relationship since a direct measurement is difficult. In the last few decades, many calibration methods are phantom-based, which determine the rigid transformation by transforming the segmented intersectional imaging region to a known phantom geometry using either point phantoms, cross-wire phantom, or plane photoms [4]. Known challenges of such phantom-based calibration include: (1) the precise phantom fabrication and assembly to ensure correct positioning of points, wires, or planes [5], and (2) unreliable recognitions of isolated points from US images [6].

B. Purpose

The objective of this study is to perform spatial calibration with multiple independent general motions and determine the known transformation parameters with a closed-form solution to a matrix equation obtained from the relative motion information.

II. Methods

A. Probe Tracking

During probe tracking, probe motion was tracked with an optical camera, OptiTrack V120: Trio (NaturalPoint, Inc.) with a frame rate of 120 Hz. The marker set consisted of five asymmtrically placed retroreflective markers which were attached to the top of the probe. The tracking system assigned a coordinate system to each marker set as a rigid body.

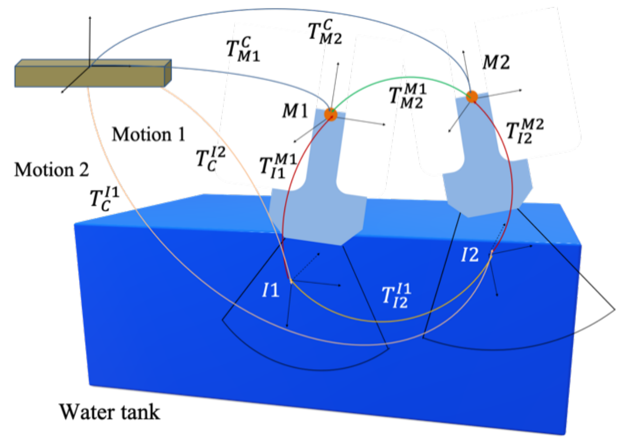

Fig. 1. Involved transformations in the proposed calibration

Fig. 1 demonstrates the involved camera coordinate system (C), marker coordinate systems (M1 and M2), image coordinate systems (I1 and I2), and transformations in the calibration via independent general motions. T_A^B denotes transformation from coordinate A to coordinate B. As shown in Fig. 1, the probe was moved from the initial location (left) to the other location (right), in which the transformation (T_{M2}^{M1}) between the before and after locations of the marker set attached to the probe could be calculated based on the camera tracking.

B. Imaging Plane Estimation

Relative frame motions of the independent general motions are also required to solve the spatial calibration problem. The most challenging issue of spatial calibration is the unavoidable and noticeable localization errors caused by the large elevation beam width determined by the size and curvature of the crystal or lens [7]. A three-point model was adopted to approach the location of the imaging plane. Two of the three points were the midpoint of the two short edges of the probe surface. To determine the third point, a 7.95 mm bead phantom was imaged at different depths with the Butterfly iQ probe (Butterfly Network, Inc.). The position where the imaging of the bead phantom was brightest was selected (Fig. 2). Once the three points were decided, they were replaced with markers to represent the location of the imaging plane. From the tracking data, the relative transformation (T_{I2}^{I1}) of the frame motion could be estimated.

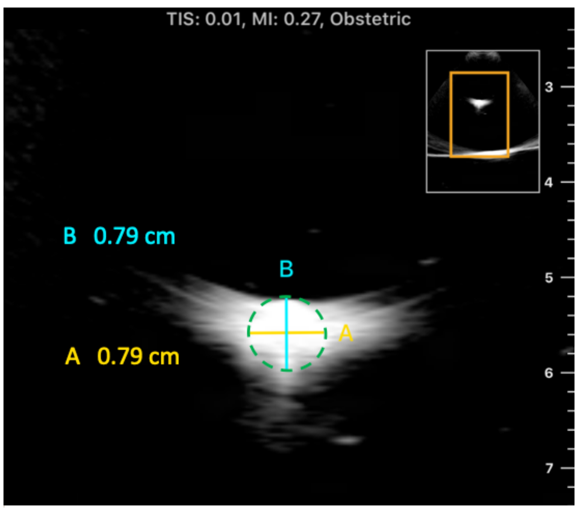

Fig. 2. B-mode image of the bead using the Butterfly iQ probe

C. Rigid Body Transformation

The rigid body transformation was solved analytically through a matrix equation ($AX = XB$) in a special form of the Sylvester equation.

Fig. 1 shows two different paths to transform the image coordinate $I2$ to the marker coordinate M1, which formed the equation $T_{M2}^{M1}T_{I2}^{M2} = T_{I1}^{M1}T_{I2}^{I1}$, where T_{I2}^{M2} and T_{I1}^{M1} were equal and represent the unknown rigid body transformation since the relative relationship between the marker set and the imaging plane is fixed. With two sets of the relative probe motion T_{M2}^{M1} (A) and the relative frame motion T_{I2}^{I1} (B) obtained from the tracked independent general probe motions as mentioned in the last two sections, the matrix equation could be solved uniquely with rotation logarithms [8]. The solution was a homogeneous transformation matrix, from which the relative six degrees of freedom (6-DoF) parameters (yaw, pitch, and roll angles for rotation, Tx, Ty, Tz for translation) could be deduced.

Probe motion consisted of both rotation and translation as general motions. Two general motions that did not share parallel axes are independent [9]. To evaluate the calibration accuracy, starting with the initial location, the probe was moved to two different locations through two independent general motions to obtain the estimated rigid body transformation. The positions and orientations were recorded by the camera of both the marker set on top of the probe and the marker set representing the imaging plane location. The camera kept tracking the subsequent freehand motion of the probe for 60 seconds for validation purpose. For each pair of captured locations of the probe and imaging plane, the transformation could be calculated based on the tracking data.

III. Results & Discussion

Theoretically, the 6-DoF relative pose deduced from each calculated transformation should be the same. However, due to the uncertainties of the tracking system, the relative poses were variant in a real situation. Table I shows the estimated pose (EST) and the average values (AVG) as the reference and standard deviation (STD) of the calculated transformations.

Table I. Statistical Analysis of Caluculated 6-DoF Poses and the Estimated Pose

	Pitch (deg)	**Yaw (deg)**	**Roll (deg)**	**Tx (mm)**	**Ty (mm)**	**Tz (mm)**
EST	-24.46	5.38	26.82	21.64	-154.10	24.26
AVG	-26.26	3.23	29.14	23.96	-151.46	34.01
STD	0.86	0.47	0.24	0.63	0.48	1.48

By comparing each calculated relative pose with the average pose, the error range for each DoF is shown in Fig. 3. Fig. 3 also demonstates the absolute errors between the estimated relative pose and the reference.

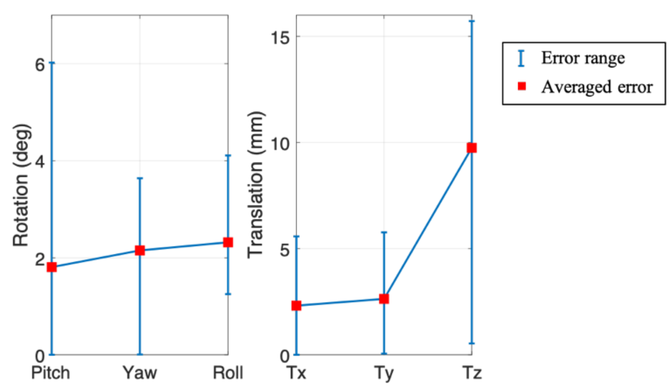

Fig. 3. 6-DoF Calibration Absolute Errors

The overall calibration achieved millimeter-level accuracy for translational and degree-level accuracy for rotational DoFs. One error source was the analytical solution of the equations, which may be improved through iterative optimization [10]. Compared with the other 5 DoFs, the error of translational position along the z-axis (Tz) was noticeable. A possible reason for this may be the tracking uncertainty along the z-axis as the z-axis is the depth direction (perpendicular to the lenses) [11]. The error range of Tz shown in Fig. 3 is almost three times greater than the other two translational DoFs, but this may be reduced with an optimized marker set configuration. Future work includes enabling the estimation of the relative frame motion during the calibration process to be less dependent upon delicately designed phantoms.

IV. Conclusion

This paper reported a spatial calibration method for 3D freehand US technique via independent general motions. With the three-point model estimating the imaging plane and two independent general probe motions, the proposed method estimated the rigid body transformation between the marker coordinate (attached to the probe) and the imaging coordinate. The overall calibration accuracies were millimeter-level for translational and degree-level for rotation DoFs. While the results are promising, they may be further enhanced with an iterative process to solve the equations and optimized marker set configurations for improved tracking.

Acknowledgment

The work was supported by Bill & Melinda Gates Foundation nder the Award OPP1191684. The authors would like to thank Butterfly Network Inc. for their support.

References

[1] Z. Chen and Q. Huang, “Real-time freehand 3D ultrasound imaging.pdf,” Comput Methods Biomechanics Biomed Eng Imaging Vis, vol. 6, no. 1, pp. 1–10, 2016, doi: 10.1080/21681163.2016.1167623.

[2] M. H. Mozaffari and W.-S. Lee, “Freehand 3-D Ultrasound Imaging: A Systematic Review.,” Ultrasound Medicine Biology, vol. 43, no. 10, pp. 2099–2124, 2017, doi: 10.1016/j.ultrasmedbio.2017.06.009.

[3] L. Mercier, T. Langø, F. Lindseth, and L. D. Collins, “A review of calibration techniques for freehand 3-D ultrasound systems,” Ultrasound Medicine Biology, vol. 31, no. 2, pp. 143–165, 2005, doi: 10.1016/j.ultrasmedbio.2004.11.001.

[4] P.-W. Hsu, R. W. Prager, A. H. Gee, and G. M. Treece, “Real-Time Freehand 3D Ultrasound Calibration,” Ultrasound Medicine Biology, vol. 34, no. 2, pp. 239–251, 2008, doi: 10.1016/j.ultrasmedbio.2007.07.020.

[5] J. Shen, N. Zemiti, J.-L. Dillenseger, and P. Poignet, “Fast And Simple Automatic 3D Ultrasound Probe Calibration Based On 3D Printed Phantom And An Untracked Marker,” Conf Proc Annu Int Conf Ieee Eng Medicine Biology Soc Ieee Eng Medicine Biology Soc Annu Conf, vol. 2018, pp. 878–882, 2018, doi: 10.1109/embc.2018.8512406.

[6] C. Shen, L. Lyu, G. Wang, and J. Wu, “A method for ultrasound probe calibration based on arbitrary wire phantom,” Cogent Eng, vol. 0, no. 0, 2019, doi: 10.1080/23311916.2019.1592739.

[7] T. K. Chen, A. D. Thurston, M. H. Moghari, R. E. Ellis, and P. Abolmaesumi, “A real-time ultrasound calibration system with automatic accuracy control and incorporation of ultrasound section thickness,” pp. 69182A-69182A–11, 2008, doi: 10.1117/12.770393.

[8] Y. C. Shiu and S. Ahmad, “Calibration of wrist-mounted robotic sensors by solving homogeneous transform equations of the form AX=XB,” Ieee T Robotic Autom, vol. 5, no. 1, pp. 16–29, 1989, doi: 10.1109/70.88014.

[9] N. Andreff, R. Horaud, and B. Espiau, “Robot Hand-Eye Calibration Using Structure-from-Motion,” Int J Robotics Res, vol. 20, no. 3, pp. 228–248, 2001, doi: 10.1177/02783640122067372.

[10] J. Wu, Y. Sun, M. Wang, and M. Liu, “Hand-Eye Calibration: 4-D Procrustes Analysis Approach,” Ieee T Instrum Meas, vol. 69, no. 6, pp. 2966–2981, 2020, doi: 10.1109/tim.2019.2930710.

[11] Q. Cai, C. Peng, J. C. Prieto, A. J. Rosenbaum, J. S. A. Stringer, and X. Jiang, “A Low-Cost Camera-Based Ultrasound Probe Tracking System: Design and Prototype,” 2019 Ieee Int Ultrasonics Symposium Ius, vol. 00, pp. 997–999, 2019, doi: 10.1109/ultsym.2019.8925631.